Axially Asymmetric Steady State Model of Jupiter's Magnetosphere-Ionosphere Coupling

I. A. Pensionerov[1], S. W. H. Cowley[2], E. S. Belenkaya[1], I. I. Alekseev[1]

[1]Federal State Budget Educational Institution of Higher Education M.V. Lomonosov Moscow State University, Skobeltsyn Institute of Nuclear Physics (SINP MSU), 1(2), Leninskie gory, GSP-1, Moscow 119991, Russian Federation
[2]Department of Physics and Astronomy, University of Leicester, Leicester, UK

Key Points:

- We develop an axially asymmetric model of Jovian magnetosphere-ionosphere coupling
- Comparison of model calculations with observed magnetodisc radial currents suggests an average radial mass transport rate of ∼2000 kg s^{-1}
- Inclusion of a nightside partial ring current significantly reduces the discrepancy between model and observed radial currents beyond 40 R_J

Corresponding author: I. A. Pensionerov, pensionerov@gmail.com

Abstract

We present an axially asymmetric steady state model of Jupiter's magnetosphere-ionosphere coupling, including precipitation-induced enhancement of the ionospheric Pedersen conductivity. We compare the magnetodisc current intensities calculated using this model with those determined directly from magnetic field measurements in various local time sectors, and find that the observed radial current intensities require an average radial mass transport rate of magnetospheric plasma of 2000 kg s^{-1}. Models with a traditional mass transport value of 1000 kg s^{-1} produce significantly weaker radial currents than observed. We also study the effect of additional field-aligned currents associated with Jupiter's nightside partial ring current and find that their inclusion leads to much better agreement between the model and observed magnetodisc radial currents in the region beyond ∼40 Jupiter radii.

1 Introduction

Jupiter has a powerful source of plasma deep within the magnetosphere in the volcanic moon Io which orbits at around 6 R_J. Here $R_J = 71492$ km is Jupiter's equatorial 1 bar radius (e.g Joy, 2002). Plasma is transported radially outward from the Io torus, and in the absence of a torque acting on the plasma its angular velocity would fall with radial distance as $1/\rho^2$ due to angular momentum conservation. However, the decrease in equatorial plasma angular velocity mapped into the ionosphere increases the collisional friction between ionospheric ions and atmospheric neutrals. In steady state this torque is balanced by the $\mathbf{j} \times \mathbf{B}$ force of the equatorward Pedersen current in the ionosphere, with the collisional torque being transferred to the equatorial magnetosphere by field-aligned currents. The equatorial plasma is then sped up towards corotation by the $\mathbf{j} \times \mathbf{B}$ force of an outward radial current which closes the current system (Hill, 1979). Figure 1 shows the overall current system enforcing corotation. The upward ionospheric field-aligned current region is associated with precipitating electrons and has been suggested to be the source of Jupiter's main oval auroral UV emissions (Cowley & Bunce, 2001; Hill, 2001).

The key parameters of the Hill (1979) model of corotation enforcement are the equatorial magnetic field profile, the plasma mass outflow rate, and the Pedersen conductivity of the ionosphere. The model has been improved and built upon for many years. Pontius (1997) used a realistic magnetic field model that takes into account the current disc field, instead of the simple dipole field used by Hill (1979) to calculate angular velocity profile. Hill (2001) and Cowley and Bunce (2001) studied the current system corresponding to the calculated angular velocity profiles and considered its connection to the auroral emissions. Nichols and Cowley (2003) studied the effect of different mass transport rates and ionospheric conductivities on the solutions, while Nichols and Cowley (2004) accounted for ionospheric conductivity modulations by precipitation associated with upward field-aligned current regions. The effect of decoupling of the magnetosphere and ionosphere due to field-aligned voltages, solar wind pressure changes, neutral flow in the ionosphere and diurnal variations of ionospheric conductivity on magnetosphere-ionosphere (M-I) coupling were studied by Nichols and Cowley (2005), Ray et al. (2010), Cowley et al. (2007), Tao et al. (2009), Ray et al. (2015), and Tao et al. (2010), respectively. Louarn et al. (2016) studied the empirical connection between auroral radio activity and the radial mass transport rate.

Azimuthal currents in the current disc are determined by radial force balance, and hence depend on the angular velocity profile, while the angular velocity profile, in turn, depends on the magnetic field created by the current disc. Nichols (2011) used the steady state model of radial force balance derived by Caudal (1986) to develop a self-consistent model of the current disc and M-I coupling. Nichols et al. (2015) further developed this model by accounting for anisotropic plasma pressure, while Nichols et al. (2020) used

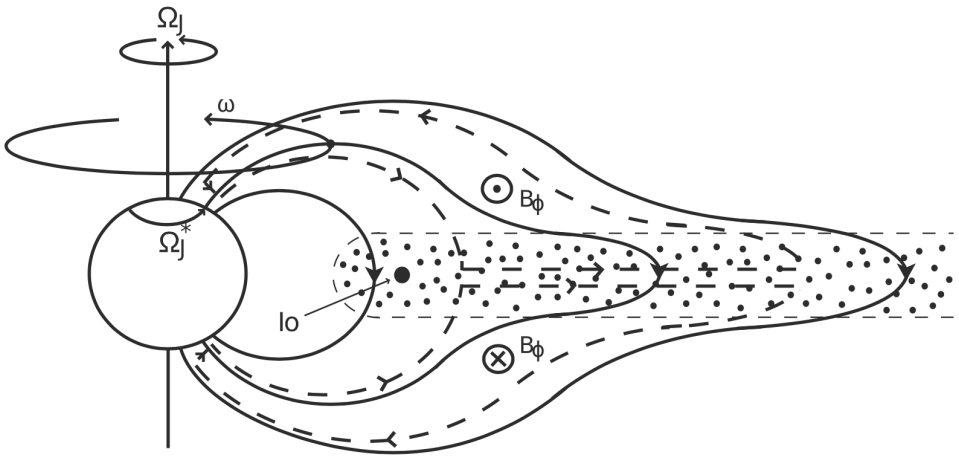

Figure 1. Sketch showing a meridian cross-section through Jupiter's magnetosphere. Arrowed solid lines show magnetic field lines. Arrowed dashed lines show the currents. Ω_J, Ω_J^* and ω are the angular velocities of Jupiter, the upper neutral atmosphere in the ionospheric Pedersen layer, and the plasma in a given flux tube, respectively. The dotted region represents the current sheet plasma. Taken from Nichols (2011), adapted from Cowley and Bunce (2001).

the model to study transient enhancements of the aurora and azimuthal and radial magnetic fields.

Ray et al. (2014) studied local time (LT) asymmetries of M-I coupling at Jupiter using the Vogt et al. (2011) empirical magnetic field model. They assumed an effective ionospheric Pedersen conductivity of 0.1 mho, constant in latitude and LT, and a mass outflow rate of 1000 kg s^{-1}. The M-I coupling model employed is axisymmetric, as used in most studies of M-I coupling based on Hill's (1979) work. Lorch et al. (2020) used magnetic field measurements obtained from all the spacecraft that have visited Jupiter to map the average radial and azimuthal current intensities in the magnetodisc in radial distance and LT. Since the radial currents are a key part of the M-I coupling current system, these observations provide an important opportunity to study LT asymmetries at Jupiter.

In this work we develop an axially asymmetric variation of the Hill (1979) model, with variable ionospheric conductivity dependent on the field-aligned current density following Nichols and Cowley (2004). We compare the model results with the currents calculated by Lorch et al. (2020), and investigate the system behavior using different mass transport rates. We find that the value 2000 kg s^{-1}, larger than usually estimated, better accounts for the observed radial currents. Lorch et al.'s (2020) results show an asymmetry of the magnetodisc azimuthal currents, which can be thought of as a partial ring current in the nightside magnetosphere. We study the effect of additional field aligned currents connected to this partial ring current on the overall M-I coupling current system, and find that their inclusion into the model significantly reduces the discrepancy between the model and the observed radial currents at distances beyond ∼40 R_J.

2 Theoretical Background

2.1 Partial Differential Equation for Angular Velocity

In this section we derive the partial differential equation for the plasma angular velocity profile, generalizing previous work to the case of axial asymmetry, thus forming a two dimensional extension of the Hill-Pontius equation (Hill, 1979; Pontius, 1997; Cowley et al., 2002). Calculation of the M-I coupling currents follows Cowley and Bunce (2001), with an angular momentum balance equation derived analogously to that given by Cowley et al. (2002), but now not assuming axial symmetry.

A simple way to map magnetically between the equatorial plane and the ionosphere is provided by Euler's potentials. A magnetic field $\mathbf{B}$ can be expressed in terms of such potentials f and g as

$$\mathbf{B} = \nabla f \times \nabla g, \tag{1}$$

where both f and g are constant along field lines because the magnetic field vector is perpendicular to their gradients. In cylindrical coordinates we assume $g = \phi$ and $f = F(\rho, \phi, z)/R_J$ and thus disregard B_ϕ. With this assumption

$$B_z = \frac{1}{\rho}\frac{\partial F}{\partial \rho}. \tag{2}$$

For purposes of modeling we consider the internal magnetic field of the planet to be dipolar, for which function F is given by

$$F_d = B_J \rho^2 \left(\frac{R_J}{r}\right)^3, \tag{3}$$

where ρ is the cylindrical distance from the magnetic axis, r is the distance from the center of the planet, and B_J is Jupiter's equatorial magnetic field strength ($B_J = 4.28 \times 10^5$ nT in the VIP4 internal field model of Connerney et al. (1998)). Near the planetary surface the internal planetary field is dominant, so that assuming the planet is approximately spherical, the ionospheric F is

$$F_i = \rho_i^2 B_J, \tag{4}$$

where ρ_i is the perpendicular distance from the magnetic axis in the ionospheric layer. Since f is constant along a field line, we can map between the magnetospheric equator and the ionosphere using

$$F_e(\rho, \phi) = F_i(\rho_i, \phi). \tag{5}$$

From current continuity, the structure of the current system shown in Figure 1, and the assumption of north-south symmetry it follows that on a given flux shell in a given azimuthal sector

$$\rho i_\rho = 2\rho_i i_P, \tag{6}$$

where i_ρ is the radial current intensity in the equatorial current disc integrated through its north-south width, and i_P is the ionospheric height-integrated Pedersen current intensity given by

$$i_P = 2B_J \rho_i \Sigma_P^* (\Omega_J - \omega). \tag{7}$$

Here we have assumed that the polar planetary field is near-vertical and of strength $2B_J$, $\Omega_J = 1.76 \times 10^{-4}$ rad s^{-1} is Jupiter's angular velocity, ω is the ionospheric plasma angular velocity, and Σ_P^* is the effective height-integrated ionospheric Pedersen conductivity. The effective conductivity accounts for rotational lagging of the neutral atmosphere relative to rigid corotation due to ion-neutral collisions, and is reduced compared to the true value by an unknown factor $0 < (1 - k) < 1$, taken to be equal 0.5 following previous work (e.g., Cowley & Bunce, 2001; Cowley et al., 2002; Nichols & Cowley, 2004). From equations (4)–(7) we obtain

$$\rho i_\rho = 4\Sigma_P^* F_e (\Omega_J - \omega). \tag{8}$$

The angular momentum per unit mass of the equatorial plasma is $\rho^2\omega(\rho,\phi)$, where ω is angular velocity. The flux of angular momentum is caused by radial transport of the plasma and its rotation around the planet. The change of angular momentum per unit time in the volume between ρ and $\rho + d\rho$ and inside the sector centered at azimuthal angle ϕ with angular width $d\phi$ is

$$dT_z = \frac{\partial(\dot{M}_\rho \rho^2 \omega)}{\partial \rho}\frac{d\phi}{2\pi} + \frac{\partial(\dot{M}_\phi \rho^2 \omega)}{\partial \phi} d\rho, \tag{9}$$

where $\dot{M}_\rho$ is the radial mass transport rate per 2π radians of azimuth (full equatorial circle), and $\dot{M}_\phi$ is the azimuthal mass transport rate per unit radial length. The Lorentz force torque per unit volume about Jupiter's center is $\mathbf{r}\times(\mathbf{j}\times\mathbf{B})$, where $\mathbf{r}$ is the position vector, $\mathbf{j}$ is the current density, and $\mathbf{B}$ is the magnetic field. The z-component of the torque acting on the plasma inside the volume element considered is

$$dT_z = -\rho^2 i_\rho B_z d\rho d\phi. \tag{10}$$

If the mass surface density of the plasma integrated through the width of the equatorial current sheet is $D(\rho,\phi)$ then

$$\dot{M}_\phi = \rho\omega D. \tag{11}$$

Substitution of equations (10) and (11) into the equation (9) gives

$$\frac{\partial(\dot{M}_\rho \rho^2 \omega)}{\partial \rho}\frac{1}{2\pi} + \rho^3 \frac{\partial(\omega^2 D)}{\partial \phi} = -\rho^2 i_\rho B_z. \tag{12}$$

We then substitute the width-integrated radial current given by equation (8) into equation (12) to obtain the following partial differential equation for the angular velocity

$$\frac{\partial(\dot{M}_\rho \rho^2 \omega)}{\partial \rho}\frac{1}{2\pi} + \rho^3 \frac{\partial(\omega^2 D)}{\partial \phi} = -4\Sigma_P^* \rho B_z F_e(\Omega_J - \omega). \tag{13}$$

Physically correct solutions must converge to almost rigid corotation close to the planet, thus the boundary condition is

$$\omega(\rho_0,\phi) \approx \Omega_J, \tag{14}$$

where ρ_0 is $\sim 6\,R_J$ (near the orbit of Io).

2.2 Modulation of Ionospheric Conductivity by Field-Aligned Currents

The ionospheric Pedersen conductivity is modulated by precipitation of electrons accelerated by field-aligned voltages in the auroral region. Nichols and Cowley (2004) calculated how the height-integrated ionospheric Pedersen conductivity depends on the ionospheric field-aligned currents density flowing out of the ionosphere, and provided the following analytic approximation

$$\Sigma_P(j_{||i}) = 0.16 j_{||i} + 2.45 \times \left(\frac{(j_{||i}/0.075)^2}{1+(j_{||i}/0.075)^2}\right) \times \frac{1}{1+\exp\left(-\frac{j_{||i}-0.22}{0.12}\right)}, \tag{15}$$

where $j_{||i}$ is the field-aligned current density just above the ionospheric layer. The effective conductivity is then

$$\Sigma_P^* = (1-k)(\Sigma_P(j_{||i}) + \Sigma_{P0}), \tag{16}$$

where Σ_{P0} is the background height-integrated ionospheric Pedersen conductivity taken to be 0.1 mho (Nichols & Cowley, 2004).

If we assume the absence of electric currents perpendicular to the magnetic field lines in the region between the current disc and the ionosphere, then $j_{||}/B$ is constant

along the field lines. Following Cowley et al. (2002) in the azimuthally symmetrical case we then find the equatorial field-aligned current density from the divergence of the radial currents

$$\frac{j_{||}}{B} = \frac{j_z}{B_e} = -\frac{1}{2B_z}\frac{1}{\rho}\frac{d}{d\rho}\left(4\Sigma_P^* F_e(\Omega_J - \omega)\right). \tag{17}$$

If there exists a partial ring current in Jupiter's magnetosphere, we should add field aligned currents associated with the divergence of the azimuthal magnetodisc currents $\nabla_\phi i_\phi$ to the equation to obtain

$$\frac{j_{||}}{B} = \frac{j_z}{B_e} = -\frac{1}{2B_z}\left(\frac{1}{\rho}\frac{d}{d\rho}\left(4\Sigma_P^* F_e(\Omega_J - \omega)\right) + \nabla_\phi i_\phi\right). \tag{18}$$

We will later define these additional field-aligned currents explicitly as an input parameter for the model. The ionospheric field-aligned current density is then

$$j_{||i} = -\frac{B_J}{B_z}\left(\frac{1}{\rho}\frac{d}{d\rho}\left(4\Sigma_P^* F_e(\Omega_J - \omega)\right) + \nabla_\phi i_\phi\right). \tag{19}$$

Equations (13) and (19) constitute a system of partial differential equations (PDEs) for ω and $j_{||i}$. Their solution requires a second boundary condition at some distance ρ_1

$$j_{||i}(\rho_1, \phi) = j_{||i0}(\phi). \tag{20}$$

Because the system of equations (13) and (19) is unstable in the near-rigid corotation region, it is very difficult to solve directly. In the next section we will discuss the reasons for this in detail and describe our approach to obtaining approximate solutions.

3 Modeling Approach

3.1 Magnetic Field Model

The model equatorial magnetospheric magnetic field employed has been derived from Galileo and Juno magnetometer data, using data from all Galileo orbits and from Juno perijoves 0–22 that are currently available. As in Lorch et al. (2020), we split the data into eight 3 h wide LT sectors, yielding sufficient data to cover radial distances of interest, and allowing us to readily compare our results with those of Lorch et al. (2020). For our purposes we are interested only in the equatorial magnetic field, so we excluded data outside of the current disc by using the Khurana (2005) current sheet model to determine when the spacecraft was farther than 0.5 R_J from the center of the sheet. We then fitted the polynomial

$$B_z(\rho) = \frac{a}{\rho} + \frac{b}{\rho^2} + \frac{c}{\rho^3} \tag{21}$$

to the z component of the residual magnetic field in each LT sector. The residual field was obtained by subtracting the JRM09 model of the internal planetary field (Connerney et al., 2018) from the data. (We note that for the modelling we still used a dipolar internal magnetic field model because of the assumed north-south symmetry and the neglect of dipole tilt). For $\rho < 10\ R_J$ we used the current disc field model developed by Pensionerov et al. (2019) instead of the polynomial given by equation (21), smoothing the transition between the two field regimes by linear interpolation. Table 1 lists the coefficients of the polynomial used in the LT sectors 00 to 21, while Figure 2 shows the resulting approximation combined with the dipolar magnetic field. Function F for this field model was then obtained by integrating equation (2).

Because we use the magnetic field model as an input for the system of equations (13) and (19), we solve it on a fine ρ grid, but in 3 h wide LT sectors. The outer boundary for our solutions is set to be at 70 R_J.

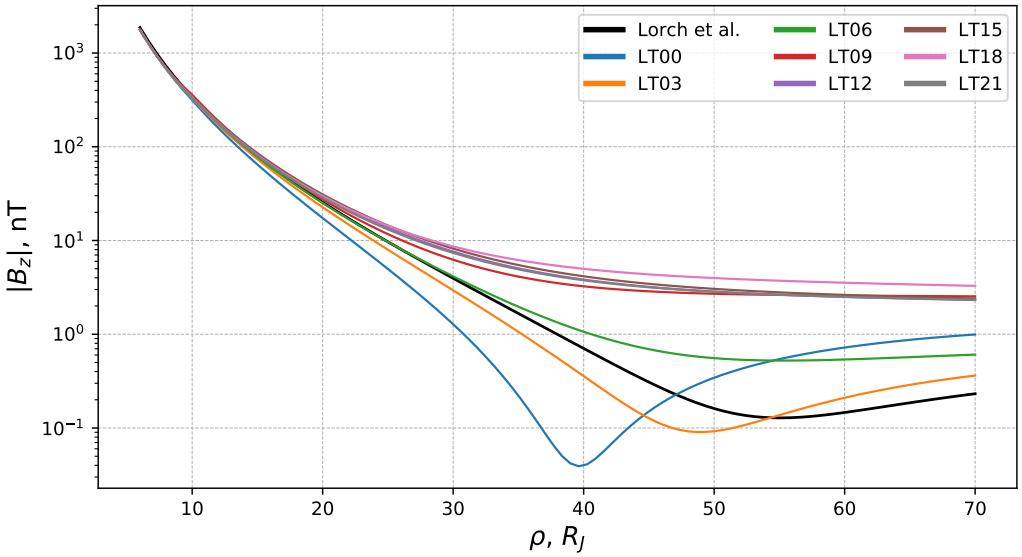

Figure 2. Absolute value of the z component of the equatorial magnetic field obtained by combining the dipolar field and the polynomial approximation of the residual magnetic field given by equation (21) with the coefficients used in the present model for LT sectors 00 to 21 h (Table 1). We also show the field profile derived by Lorch et al. (2020) also listed in Table 1.

Table 1. Coefficients of the polynomial given by equation (21), fitted to the residual z component of the equatorial magnetic field in LT sectors 00 to 21 h. Coefficients used by Lorch et al. (2020) are shown for comparison.

LT	a, $10^2 \cdot$ nT	b, $10^4 \cdot$ nT	c, $10^4 \cdot$ nT
00	-3.620	2.854	-13.891
03	-2.258	2.146	-9.401
06	-2.263	2.022	-8.894
09	-4.535	2.780	-16.823
12	-3.600	2.127	-9.396
15	-3.559	2.048	-8.969
18	-4.577	2.344	-9.873
21	-3.611	2.108	-8.048
Lorch et al.	-1.825	1.893	-8.441

3.2 Method for Obtaining Numerical Solutions

Most of the Hill-Pontius differential equation solutions quickly diverge to very large positive or negative values of angular velocity in the inner magnetosphere. The physically correct solution converges to $\sim \Omega_J$. In the one-dimensional case with an explicitly defined ionospheric conductivity function $\Sigma_P^*(\rho)$, the solution can easily be obtained by solving the equation radially outward with the boundary condition $\omega(\rho_0) = \Omega_J$, where ρ_0 is several R_J. This is because solutions with slightly different boundary conditions near the planet quickly converge to the one solution we are interested in as shown in the appendix of Cowley and Bunce (2003).

This approach cannot be applied to the Hill-Pontius equation combined with the equation for ionospheric conductivity modulation by field-aligned currents, because it becomes unstable in the inner region. Since we cannot start the solution from the rigid corotation region, we cannot ensure the fulfillment of the boundary condition equation (14) by solving the equations radially outward. Nichols and Cowley (2004) deal with this problem by solving the equations radially inward. They fixed the field-aligned current at a distance of $100\,R_J$ and used a binary search to find the value of the angular velocity that leads approximately to rigid corotation near the planet, by tracing the solution inward. A binary search is allowed by the fact that the solutions diverge to large positive values for boundary angular velocities above the correct one and to large negative values for those below. This method requires the angular velocity boundary condition to be specified to a large number of digits. Nichols and Cowley (2004) traced the solution to 10–20 R_J and used an approximate iterative solution in the inner region. The same can be done with a fixed angular velocity and binary-searched field-aligned current boundary condition.

The method for solving the one dimensional Hill-Pontius equation with an explicit conductivity can easily be adapted to the two dimensional case. However, the Nichols and Cowley (2004) method for solving the equation with variable conductivity cannot be translated to the partial differential equations developed here because a binary search of the second boundary condition becomes impossible due to the influence of the azimuthal sectors on each other. The crux of the issue lies in the second term of equation (13) that accounts for the net azimuthal transport of angular momentum $\rho^3 \frac{\partial(\omega^2 D)}{\partial \phi}$. It is useful, therefore, to estimate the significance of this term in comparison with the other terms. For this purpose, as well as later for obtaining the solutions, we need an estimate of the plasma mass density. For this purpose we employed the profile of cold plasma concentration per unit magnetic flux from Nichols (2011), which together with our magnetic field model yields the number density, and hence the mass density assuming an average ion mass of 20 amu.

To estimate the significance of azimuthal transport we used the Hill (1979) analytical angular velocity profile applicable in case of a purely dipolar magnetic field, because it is generally representative of the plasma angular velocity behavior at Jupiter. We also assumed an upper bound for the azimuthal derivative of ω to be $0.5 \times (\Omega_J - \omega)$, consequent on the fact that as the angular velocity converges towards rigid corotation, its azimuthal derivative should converge towards zero. The choice of the coefficient 0.5 is based on the comparison of angular velocity profiles obtained by solving the one-dimensional system of equations for each LT separately. Finally, the azimuthal derivative of the mass density was for simplicity assumed to be zero, noting the lack of detailed LT-dependent density measurements. Using these assumptions we compared the electromagnetic torque (the right hand side of equation (13)) with the azimuthal transport term. Figure 3 shows a comparison using Hill's solution with a characteristic distance $\rho_H = 25\,R_J$ (the distance at which the angular velocity starts to deviate significantly from rigid corotation). The result varies with the plasma density and ρ_H, but in most cases the azimuthal angular momentum transport effect is at least several times less than the electromagnetic torque effect in the region $\rho < 25\,R_J$. Thus in the absence of a bet-

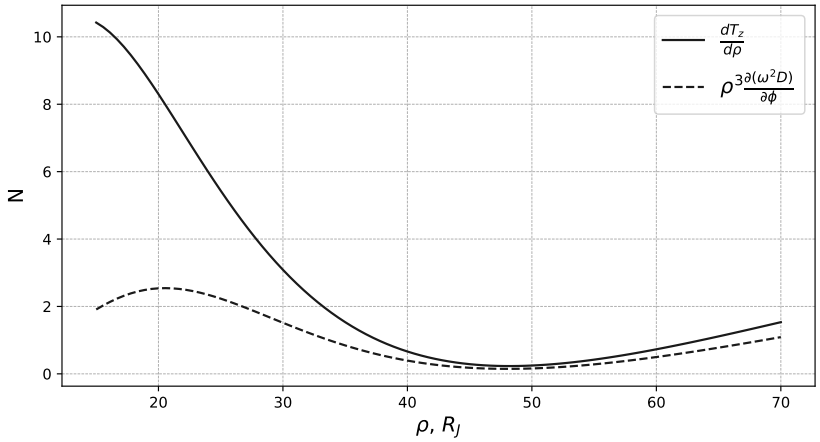

Figure 3. Comparison of terms in equation (13), where the solid line shows the electromagnetic torque term while the dashed line shows an estimate of the net azimuthal transport of angular momentum term.

ter approach we neglect the second term in equation (13) and solve the system of equations (13) and (19) for each LT sector radially inward using the Nichols and Cowley (2004) method.

After obtaining the boundary values for ω and $j_{||i}$ at $\rho = 25\,R_J$ which correspond to a solution that converges to approximately Ω_J in the inner region, we can use these boundary conditions to solve the system of equations (13) and (19) radially outward in the case without net azimuthal angular momentum transport. This approach usually yields a valid solution, though, depending on the magnetic field profile and the chosen fixed boundary condition, it can produce a solution for field-aligned currents that diverges to large positive values. However, as shown in Figure 3, the azimuthal transport is not necessarily negligible in the region $\rho > 25\,R_J$. Unfortunately, solving the system of equations (13) and (19) with inclusion of net azimuthal transport often leads to diverging solutions, rendering this approach very difficult to implement reliably. Thus, to solve the equation in the region $\rho > 25\,R_J$ we need further simplification.

We propose the following approach. We solve the one-dimensional problems with variable ionospheric conductivity for each sector radially outward, neglecting net azimuthal transport of angular momentum. We then treat the conductivities calculated from the one-dimensional solutions as explicitly defined and use them to solve equation (13) radially outward, this time accounting for azimuthal transport in the $\rho > 25\,R_J$ region. We effectively account for the influence of field-aligned currents on the conductivity and the contribution of azimuthal angular momentum transport sequentially, instead of solving an equation that accounts for both of them simultaneously. In justification of this method we can offer our results obtained from our attempts to solve the partial differential equations taking account of azimuthal transport and variable conductivity simultaneously. As indicated above, this approach was deemed too unreliable to be used in the final implementation. However, the successful solutions demonstrated little change in the resulting conductivity, compared with the equivalent solutions obtained without azimuthal transport.

3.3 Boundary Conditions

As stated above, the Nichols and Cowley (2004) method of solving the Hill-Pontius equation with variable conductivity requires one of the boundary conditions to be fixed, while the other is found by tracing solutions radially inward and binary searching the value that leads to near-rigid corotation in the inner region. To solve our equation we need to set boundary conditions for each of the LT sectors at $\rho = 25\,R_J$. We do not know the angular velocity or the field-aligned currents, but we have the radial current observations derived by Lorch et al. (2020). With these values and equations (8) and (16) we have a connection between the boundary conditions

$$i_\rho(\omega_0, j_{||i0}) = i_\rho^{(\text{observed})}. \tag{22}$$

We then can binary search pairs of ω and $j_{||i}$ until we find boundary conditions which lead to a physically correct solution, by selecting a value of $j_{||i}$ and computing ω from equation (22) on each iteration. Not every value of radial current has a solution converging to near-rigid corotation. The deciding factor in whether or not such a solution exists for a given boundary radial current is the value of $\dot{M}_\rho$. For example, with $\dot{M}_\rho = 1000$ kg s^{-1} the observed radial currents are typically too large and the equation has no physically correct solutions. In such cases we iteratively decreased the boundary radial currents from the observed value until a valid solution became possible.

3.4 Algorithm Outline

The final algorithm for obtaining solutions to the system of equations (13) and (19) is as follows.

1. We trace the solutions radially inward from $\rho = 25\,R_J$. We binary search pairs of boundary conditions for angular velocity and ionospheric field-aligned current density that satisfy equation (22) and correspond to a solution that converges to approximately rigid corotation near the planet. In cases where such a solution does not exist for a given boundary radial current, we iteratively decrease the boundary currents, conducting a new binary search for each iteration, and repeating the procedure until a solution is found. The search is conducted separately for each LT sector under the assumption that the effect of net azimuthal angular momentum transfer is negligible in that region.
2. The solutions in the previous step are traced to 15 R_J. Tracing to the region closer to the planet becomes too computationally intensive. To obtain the solution in the region from 6 to 15 R_J we interpolate the field-aligned currents at the 15 R_J boundary to zero at 10 R_J using a cubic spline. We then calculate the corresponding ionospheric conductivity and use it explicitly to solve the simple Hill-Pontius equation radially outward in the 6 to 15 R_J region. Because the field-aligned currents at 15 R_J are comparatively small, the combined solution from this step and the previous one is continuous.
3. We solve the system radially outward from 25 to 70 R_J. The azimuthal angular momentum transfer effect in this region is not negligible. However, we still solve the equations for each LT sector separately, thus neglecting it. We account for the azimuthal transport to some extent in the next step.
4. We use the field-aligned currents obtained in the previous step to calculate the ionospheric conductivity for each LT sector. We then use these conductivities explicitly to solve equation (13) radially outward from 25 to 70 R_J, accounting for the net azimuthal angular momentum transfer effect.
5. The full solution is constructed from those obtained in steps 1, 2 and 4.

4 Results

4.1 Solutions Without Field-Aligned Currents from the Partial Ring Current

We now examine the solutions obtained using the method described in section 3.4, and compare the model magnetodisc radial current intensities with those determined by Lorch et al. (2020). The key model parameter is the radial mass transport rate $\dot{M}_{\rho}$. For simplicity we assume it to be symmetrical in LT and constant with ρ. In reality, $\dot{M}_{\rho}$ likely becomes asymmetric within the radial distance range of interest, but we leave the examination of such asymmetry effects for future work. Here we compare solutions for the canonical $\dot{M}_{\rho}$ value of 1000 kg s^{-1}, and an increased value of 2000 kg s^{-1}.

In Figure 4 we compare the width-integrated radial current intensities calculated from the model results for $\dot{M}_{\rho} = 1000$ kg s^{-1} (blue lines) and 2000 kg s^{-1} (orange) with the observed current intensities from Lorch et al. (2020) (black) in the LT sectors from 00 to 21 h. In the region closer than $\sim 15\,R_J$ in some sectors the observed radial currents become negative, most prominently at 21, 00/24, and 03 h. The model radial currents converge to zero near the planet, hence not accounting for the effect causing this observed behavior. At larger distances up to $\rho \sim 40\,R_J$ the observed radial current is significantly underestimated by the $\dot{M}_{\rho} = 1000$ kg s^{-1} model in most LT sectors, while the 2000 kg s^{-1} model does a noticeably better job. In the 06, 09 and 18 h sectors the model underestimates the currents with both values, with the 2000 kg s^{-1} model coming closer to the observed values. Only in the 12 h LT sector do both model variants overestimate the currents. Beyond $40\,R_J$, the behavior of the observed currents changes depending on the LT. In the midnight-dawn sector the radial current intensities tend to decrease with radial distance very slowly, while in the dusk sector and at 09 h they decrease significantly faster. It should be noted that the 09 h sector has much less spacecraft trajectory coverage over the years, with no data obtained from either Juno or Galileo beyond 40–50 R_J, such that the radial currents calculated by Lorch et al. (2020), as well as our magnetic field model, might be less reliable in this sector than in the others. The model currents are generally more similar to the observed currents in the dawn sector than in the dusk sector.

Generally in the region closer than $40\,R_J$ the model with $\dot{M}_{\rho} = 2000$ kg s^{-1} offers a reasonable approximation to the observed radial currents in most LT sectors, while the model with $\dot{M}_{\rho} = 1000$ kg s^{-1} has radial currents significantly lower than those observed. Beyond $40\,R_J$ neither model work well, with the most prominent discrepancies appearing in the dusk sector. In the following section we will attempt to improve the model by incorporating field aligned currents from the partial ring current into the calculations.

Figure 5 demonstrates the angular velocities, ionospheric field-aligned currents, and effective conductivity for the 2000 kg s^{-1} and 1000 kg s^{-1} cases. Angular velocities in the case of 2000 kg s^{-1} start to deviate significantly from rigid corotation slightly closer to the planet than for the case of 1000 kg s^{-1}, thus producing stronger radial currents. In both cases the angular velocities in the dawn sector tend to fall faster than in the dusk sector. The ionospheric field-aligned currents and conductivity behave similarly for both radial mass transport values. Field-aligned currents are typically in the range 0.1–0.2 μA m^{-2}, with peaks in the dawn sector at 20–30 R_J reaching 0.4–0.6 μA m^{-2}. The corresponding effective conductivities range from 0.1 to 1.5 mho.

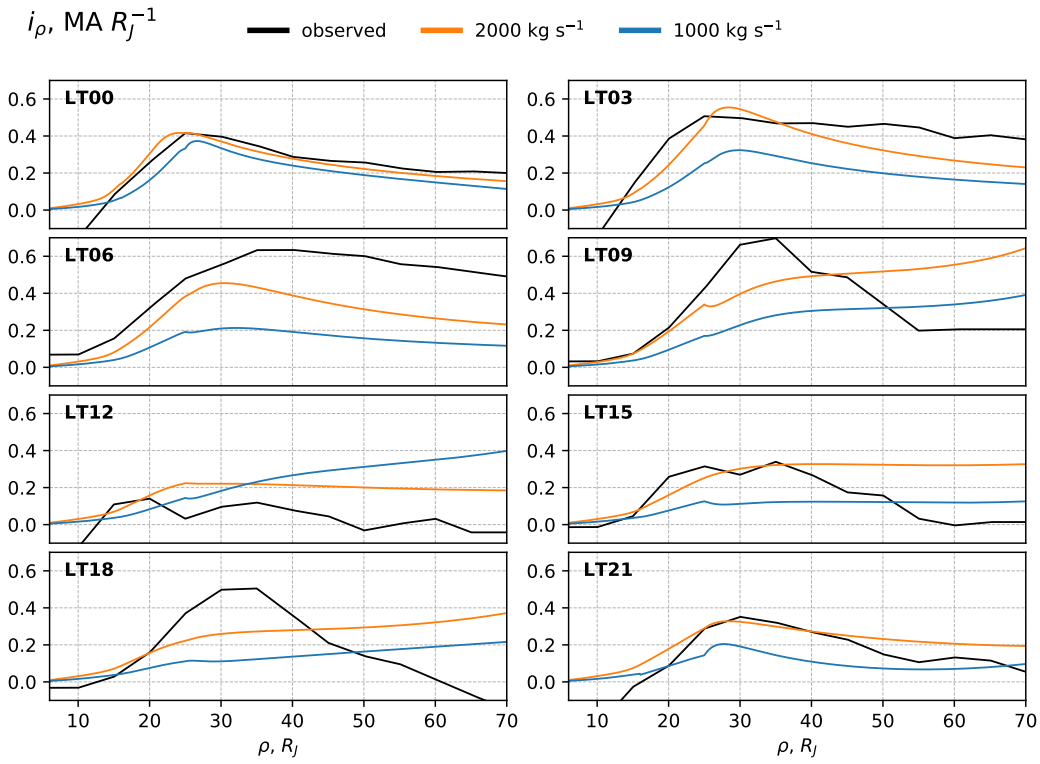

Figure 4. Equatorial width-integrated radial current intensities plotted versus distance ρ from the planetary magnetic axis in 3 h wide LT sectors LT 00–LT 21 h. Black lines show the empirical currents derived from magnetic field data by Lorch et al. (2020), while the blue and orange lines show model currents for $\dot{M}_\rho = 1000$ kg s^{-1} and $\dot{M}_\rho = 2000$ kg s^{-1}, respectively.

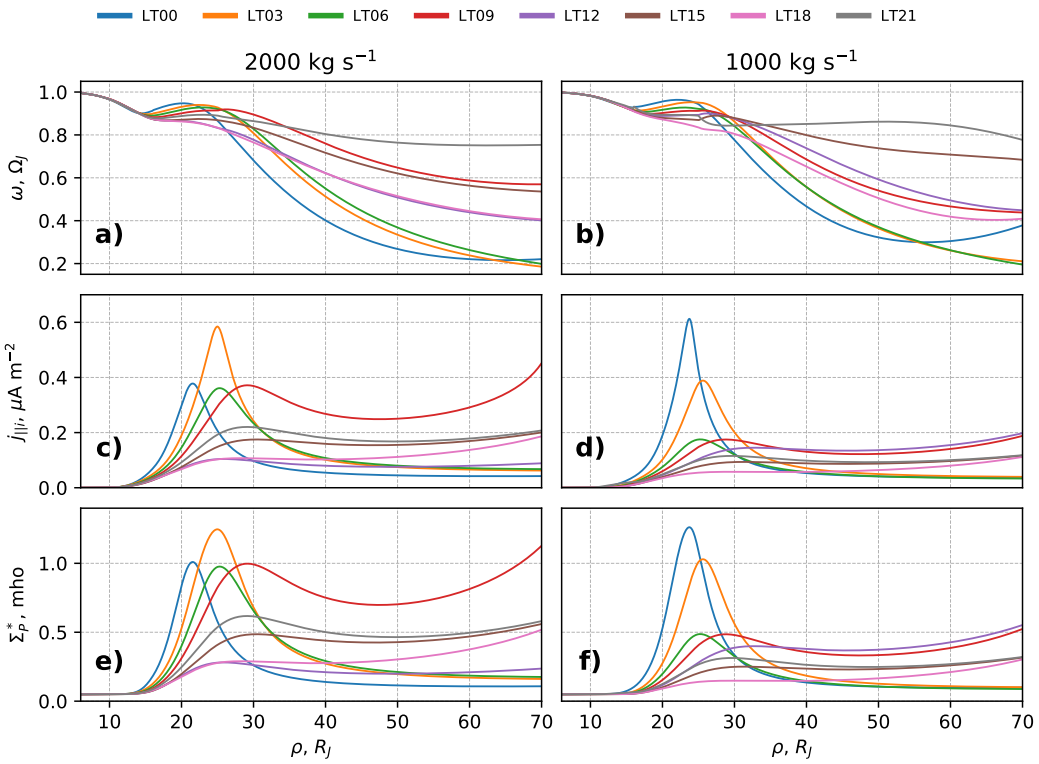

Figure 5. Panels (a) and (b) show angular velocities, (c) and (d) ionospheric field-aligned current densities, and (e) and (f) effective height-integrated ionospheric conductivities, for each LT sector. Panels on the left correspond to a mass transport rate of 1000 kg s^{-1}, while the panels on the right correspond to 2000 kg s^{-1}. All parameters are plotted versus equatorial distance from the planetary rotation axis, mapped along field lines in the case of the ionospheric parameters in panels (c)–(f).

Table 2. Parameters A and ρ_c of the approximate form for the ionospheric field-aligned currents associated with the partial ring current given by equation (23), as employed in LT sectors 00 to 21 h for the models with radial mass outflow rates of 2000 kg s^{-1} and 1000 kg s^{-1}

LT	2000 kg s^{-1}		1000 kg s^{-1}	
	A, μA m^{-2}	ρ_c, R_J	A, μA m^{-2}	ρ_c, R_J
00	0.00	30	0.00	30
03	-0.05	30	-0.05	30
06	-0.10	30	-0.10	30
09	0.00	30	0.00	30
12	0.00	30	0.00	30
15	0.07	30	0.00	30
18	0.10	35	0.00	30
21	0.05	35	0.00	35

4.2 Solutions with Field-Aligned Currents from the Partial Ring Current

Lorch et al. (2020) have calculated the divergence of their empirical azimuthal equatorial current, which ideally should be used directly in our model. However, several factors make this difficult. The solutions of the Hill-Pontius equation with variable conductivity are very sensitive not only to the magnitude of the additional field-aligned currents associated with these divergences, but also to their radial derivatives. The observed azimuthal current divergences vary significantly from one bin to the next due to statistical errors, which makes their derivatives unusable. In addition, when these divergences are projected into the ionosphere for some LTs, they cause ionospheric field-aligned currents 10–50 times larger than the typical model values derived from the divergence of the radial currents. Use of the observed divergences usually renders the equations unsolvable. Thus instead of using the observed divergences directly we employed a simple parametric equation for the additional field-aligned currents as follows

$$(\nabla_\phi i_\phi)_i = A\rho_c \frac{\tanh\left(\frac{\rho-\rho_c+d}{d}\right)+1}{\rho+\rho_c}\,. \tag{23}$$

Parameter d was set to be $5\,R_J$, while the chosen values of ρ_c and A for each LT are presented in Table 2. This equation smoothly interpolates to zero at distances smaller than ρ_c (as we assume the azimuthal currents become symmetrical in the inner magnetosphere) and its absolute value falls as $1/\rho$ at greater distances (assuming the divergence becomes smaller as the azimuthal currents themselves become smaller). The form of the approximation is somewhat arbitrary, so we only aim to qualitatively study the effects of the additional field-aligned currents. We assumed magnitudes of these field-aligned currents consistent with the data from 09 to 21 h LT, and ignored the large values in the 00 to 06 h sector. According to Lorch et al. (2020), the azimuthal current is removed from the magnetodisc in the dawn sector and added back to it in the dusk sector, and we follow this pattern in our parametric approximations. The specific values of ρ_c and A were chosen to best fit the observed radial currents with the model ones. For the 1000 kg s^{-1} model we have not included additional field-aligned currents in the dusk sector, since values consistent in direction with the observations did not improve the fits. Figure 6 shows an example of field-aligned currents at 15 h LT calculated using equation (23) with parameters for the 2000 kg s^{-1} model (solid line), together with the field-aligned currents calculated from observations (dashed line). Inside $20\,R_J$ the azimuthal current divergence was not taken into account due to relatively large errors, and was linearly interpolated

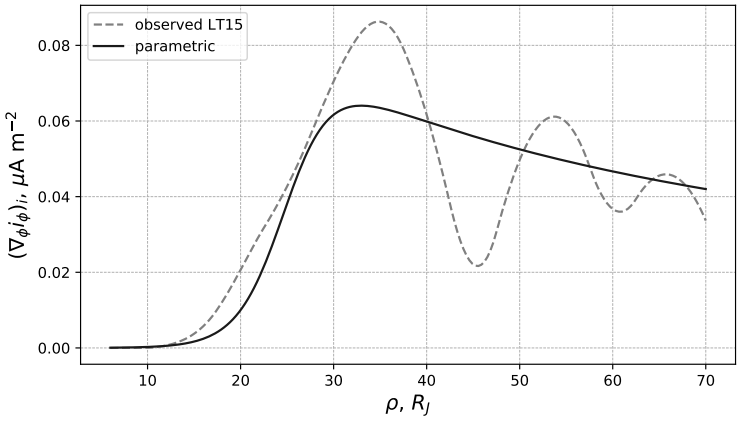

Figure 6. Field aligned current from the partial ring current plotted versus distance from the magnetic axis for 15 h LT. The solid line shows the parametric approximation given by equation (23) with $A = 0.07\ \mu\mathrm{A\,m^{-2}}$, $\rho_c = 35\ R_J$ corresponding to the 2000 kg s^{-1} case in Table 2, while the dashed line shows the field-aligned current calculated from the observed currents.

to zero from the boundary value. Beyond $20\,R_J$ the observed divergence was interpolated by quadratic splines.

Figure 7 shows the radial currents in the same format as Figure 4, but with field-aligned currents from the partial ring current included. Negative additional field-aligned currents in the dawn sector make the model radial currents in the $\rho > 40\,R_J$ region larger, bringing them closer to the observed values, especially for the 1000 kg s^{-1} model, though 2000 kg s^{-1} still gives a closer fit. Positive additional field-aligned currents in the dusk sector, on the other hand, make the model radial currents in outer region lower. This helps to significantly reduce the discrepancies between model and observations for the 2000 kg s^{-1} case. However, it still doesn't fit the observed drop to very small or even negative values in the 15 and 18 h LT sectors. In the 1000 kg s^{-1} case additional positive field-aligned currents cannot improve the performance of the model, because it underestimates the currents even without additional positive field-aligned currents. As was indicated above, 09 h LT is probably anomalous due to the limited data coverage, while 12 h LT is also not fitted well, probably because the radial mass transport rate there is even lower than 1000 kg s^{-1} for most radial distances. Overall, with inclusion of field-aligned currents from the partial ring current the 2000 kg s^{-1} model gives a reasonable fit to the observed radial currents at most LTs. While improved in the dawn sector, the 1000 kg s^{-1} model still gives a significantly worse fit compared to the 2000 kg s^{-1} model.

Figure 8 demonstrates the angular velocities, ionospheric field-aligned currents, and effective conductivity in the same format as Figure 5, but for the model with field-aligned currents from the partial ring current. The behavior and the typical values of the angular velocities, the total ionospheric field-aligned currents and conductivities are overall the same, as in the case without additional field-aligned currents.

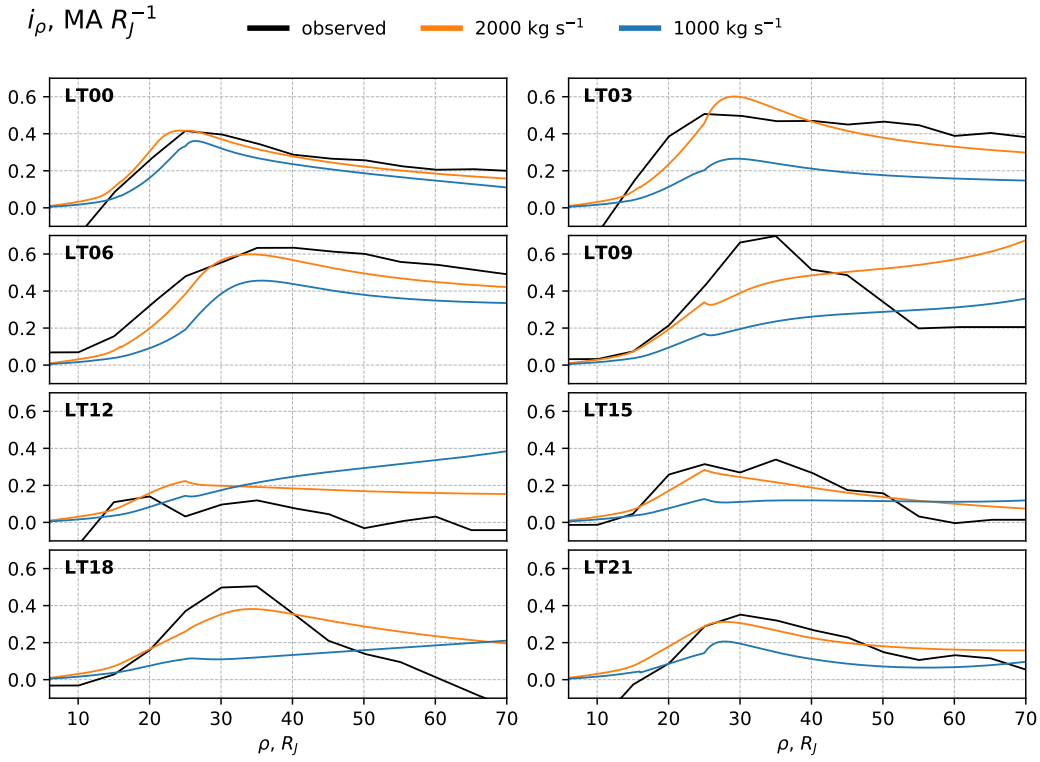

Figure 7. Same as Figure 4, but for the models including field-aligned currents from the partial ring current.

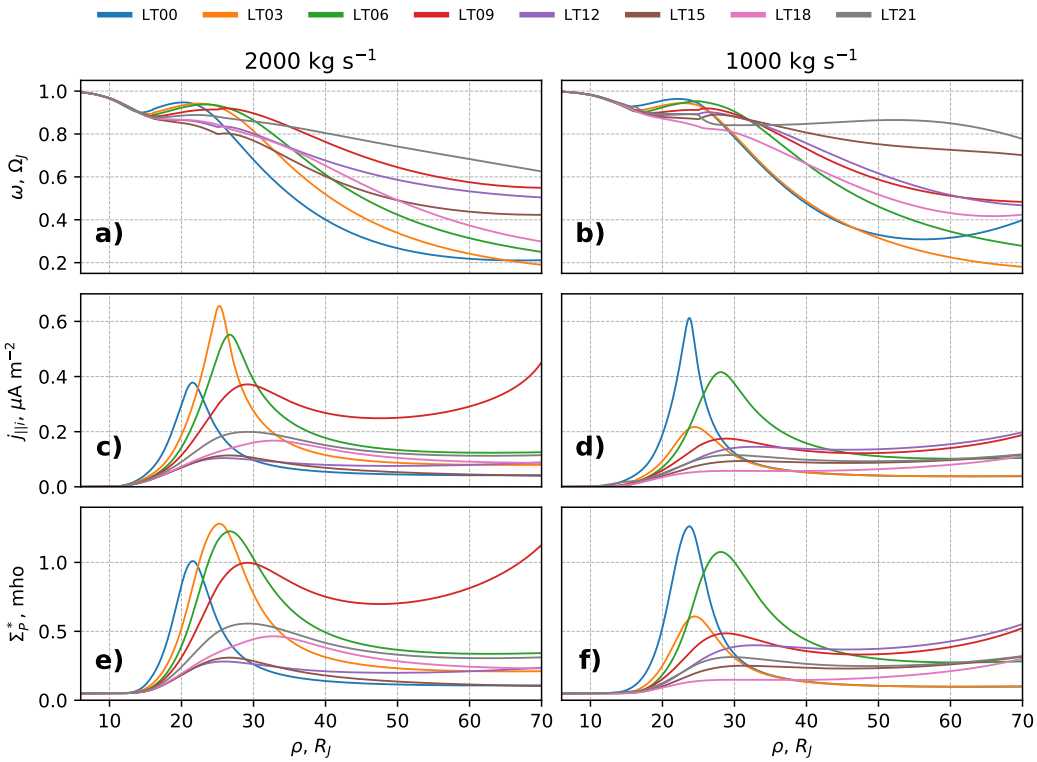

Figure 8. Same as Figure 5, but for the models including field-aligned currents from the partial ring current.

5 Discussion

A key feature of steady state M-I coupling models is their relative simplicity, compared to full 2D or 3D MHD modelling. This simplicity allows one to relatively easily with low iteration time and computing power requirements test the response of the system to different values of various parameters and compare the results with observations. Here we have developed a variation of this model which is asymmetrical in LT. This allowed us to compare the radial equatorial current densities calculated using the model with those determined from magnetic field measurements by Lorch et al. (2020) in eight 3 h wide LT sectors centered on 00 to 21 h.

The radial mass outflow rate in Jupiter's magnetosphere is a key parameter of the model, generally assumed to be equal to the Io plasma production rate. Various empirical estimates of the plasma production rate have been made, ranging from 150 to 2000 kg s^{-1} (Broadfoot et al., 1981; Vasyliunas, 1983; Bagenal, 1997; Bagenal & Delamere, 2011), and the canonical value of 1000 kg s^{-1} has been used in many previous related works (Cowley & Bunce, 2001; Cowley et al., 2002; Nichols, 2011; Ray et al., 2014; Nichols et al., 2015). Nichols et al. (2020) used the canonical value as representative of the typical outflow rate, while using 2350 kg s^{-1} for an enhanced plasma production case. Hill (2001) used the value of 2000 kg s^{-1} in his calculations, while Nichols and Cowley (2003) studied solutions of the Hill-Pontius equation for various outflow rates from 100 to 10000 kg s^{-1}. In this work we compared the equatorial radial currents produced by the model using radial mass outflow rates of 1000 and 2000 kg s^{-1}, and found that the model currents are in significantly better agreement with observations when a transport rate of 2000 kg s^{-1} is used. Currents produced in the 1000 kg s^{-1} case are systematically lower than those observed.

The magnetic field observations used by Lorch et al. (2020) to calculate the currents, and those employed by us to construct our model of the magnetospheric equatorial field, are taken from observations made on the trajectories of several spacecraft, thus representing a time-averaged picture. Thus the mass transport rates used in our modelling are taken to correspond to the average mass transport rate in the system. The value of 2000 kg s^{-1} favored by our comparison with observations is on the higher side of most estimates of Io plasma production rate. It is sometimes considered as an enhanced value, but the average value is usually estimated to be lower. Nichols and Cowley (2004) compared their calculated radial currents with those derived from Galileo azimuthal magnetic field data obtained in the midnight LT sector, and found that the model currents better fit the observed values with $\dot{M}_\rho$ set to a larger value of 2000 or 3000 kg s^{-1}. We used the same approximation for the conductivity dependence on the field-aligned ionospheric current density as Nichols and Cowley (2004), as well as the same atmosphere slippage coefficient of 0.5, which affects the effective conductivity. Preliminary tests with a lower slippage coefficient and hence higher effective conductivity did not show an increase in the model radial currents, while tests with a higher coefficient and consequent lower effective conductivity showed decreased currents. Consequently, changes in the slippage coefficient do not fix the systematic underestimation of the observed currents by the 1000 kg s^{-1} model. However, more rigorous study is needed of the behavior of the solutions with different approximations for the conductivity dependence on the field aligned current.

We also considered the effects on the solutions of field-aligned currents from the partial ring current. Because of the sensitivity of the solutions to the radial derivatives of the divergence of the equatorial azimuthal current, we were unable to use the observed divergences directly. Instead we used a simple analytic form for the resulting ionospheric field-aligned currents with parameters individually selected for each LT sector. The direction of the field-aligned currents we used is in agreement with the observations of Lorch et al. (2020). The inclusion of these currents in the model allowed us to significantly im-

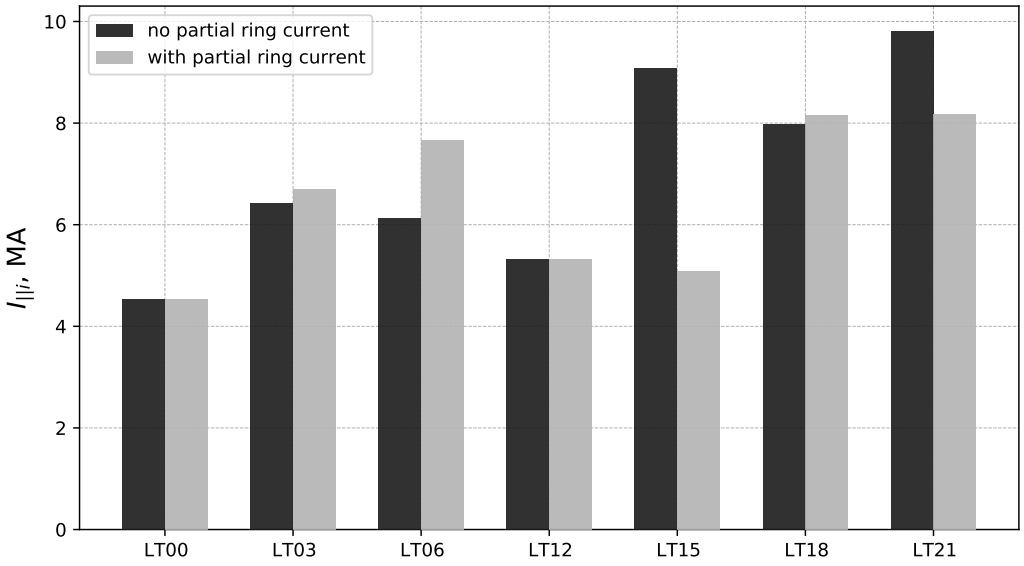

Figure 9. Upward field-aligned currents integrated over the ionosphere in one hemisphere for each 3 h wide LT sector (excluding the 09 h LT sector due to apparent inaccuracies in the magnetic field model). Black and gray bars show results without and with field aligned currents from the partial ring current, respectively. In both cases a 2000 kg s^{-1} mass outflow rate is used.

prove the agreement between the observed and model equatorial radial currents in the region beyond $\sim 40\,R_J$ from the planet.

Bonfond et al. (2015) used HST images to estimate the brightness asymmetry of the main oval of Jupiter's UV aurora. They found that in the southern hemisphere the dusk sector emission is on average ~ 3 times brighter than in the dawn sector, while in the northern hemisphere the dusk sector is only ~ 1.1 times brighter (possibly due to the northern magnetic anomaly complicating the analysis). As a possible explanation of this asymmetry, Bonfond et al. (2015) suggested the presence of a partial ring current in the nightside magnetosphere, whose field aligned currents would strengthen the main oval aurora at dusk while weakening it at dawn. The calculations by Ray et al. (2014) are inconsistent with the Bonfond et al. (2015) results, since they predict stronger field aligned currents in the dawn sector. Our calculations also show stronger field-aligned currents in the dawn sector. However, the total upward field-aligned current is not larger in the dawn sector, because in the dusk sector it covers a significantly wider latitude range. Figure 9 shows the upward field-aligned current integrated over the ionosphere in one hemisphere for each of the 3 h wide LT sectors, except for 09 h LT. The total current in this sector is approximately twice as large as in the other sectors, probably caused by an inaccurate magnetic field model due to the lack of data in the outer magnetosphere. Figure 9 shows our results for cases with and without additional field aligned currents from the partial ring current. In both cases there is no strong dawn-dusk asymmetry. We should note that the additional field-aligned currents from the partial ring current do not necessarily affect the aurora in the simple way suggested by Bonfond et al. (2015). Additional field-aligned currents change the conductivity of the ionosphere, which in turn changes the angular velocity profile, and hence the field aligned currents from the divergence of the radial currents. In the 15 and 21 h LT sectors, which have positive additional currents, the total positive field aligned current is less than in the case without additional currents, while in the 03 and 06 h LT sectors, which have negative additional

currents, the total is larger. The resulting field-aligned currents depend strongly on the magnitude and radial derivative of the additional currents.

6 Conclusions

We have presented an axially asymmetrical variant of the steady state M-I coupling model for the Jovian magnetosphere, and have compared the radial magnetodisc currents calculated using this model with those derived by Lorch et al. (2020) from in situ magnetic field observations. We found that the observed radial current magnitudes require an average radial mass transport rate of 2000 kg s^{-1}, significantly higher than the value typically used of 1000 kg s^{-1}. We also considered the effect of field-aligned currents associated with the nightside partial ring current on the M-I coupling system, and found that their inclusion results in reduced discrepancies between the model and the observed radial magnetodisc currents at radial distances beyond 40 R_J.

Acknowledgments

Authors acknowledge the support of Ministry of Science and Higher Education of the Russian Federation under the grant 075-15-2020-780 (N13.1902.21.0039). Work at the University of Leicester was supported by UKRI/STFC Consolidated Grant ST/N000749/1. Magnetometer data used in this work were retrieved from the Planetary Data System database (`https://pds-ppi.igpp.ucla.edu/`).

References

Bagenal, F. (1997). The ionization source near io from galileo wake data. *Geophysical Research Letters*, *24*(17), 2111–2114. Retrieved from `https://doi.org/10.1029/97gl02052`

Bagenal, F., & Delamere, P. A. (2011). Flow of mass and energy in the magnetospheres of jupiter and saturn. *Journal of Geophysical Research: Space Physics*, *116*(A5). Retrieved from `https://doi.org/10.1029/2010ja016294`

Bonfond, B., Gustin, J., Gérard, J.-C., Grodent, D., Radioti, A., Palmaerts, B., ... Tao, C. (2015, October). The far-ultraviolet main auroral emission at jupiter - part 1: Dawn-dusk brightness asymmetries. *Annales Geophysicae*, *33*(10), 1203–1209. Retrieved from `https://doi.org/10.5194/angeo-33-1203-2015`

Broadfoot, A. L., Sandel, B. R., Shemansky, D. E., McConnell, J. C., Smith, G. R., Holberg, J. B., ... Bertaux, J. L. (1981). Overview of the voyager ultraviolet spectrometry results through jupiter encounter. *Journal of Geophysical Research: Space Physics*, *86*(A10), 8259–8284. Retrieved from `https://doi.org/10.1029/ja086ia10p08259`

Caudal, G. (1986). A self-consistent model of Jupiter's magnetodisc including the effects of centrifugal force and pressure. *Journal of Geophysical Research*, *91*(A4), 4201.

Connerney, J. E. P., Acuña, M. H., Ness, N. F., & Satoh, T. (1998, June). New models of jupiter's magnetic field constrained by the io flux tube footprint. *Journal of Geophysical Research: Space Physics*, *103*(A6), 11929–11939. Retrieved from `https://doi.org/10.1029/97ja03726`

Connerney, J. E. P., Kotsiaros, S., Oliversen, R. J., Espley, J. R., Joergensen, J. L., Joergensen, P. S., ... Levin, S. M. (2018). A new model of Jupiter's magnetic field from Juno's first nine orbits. *Geophysical Research Letters*, *45*(6), 2590–2596. Retrieved from `https://doi.org/10.1002/2018gl077312`

Cowley, S. W. H., & Bunce, E. (2001). Origin of the main auroral oval in jupiter's coupled magnetosphere-ionosphere system. *Planetary and Space Science*, *49*(10-11), 1067–1088. Retrieved from `https://doi.org/10.1016/s0032-0633(00)00167-7`

Cowley, S. W. H., & Bunce, E. J. (2003, January). Modulation of jovian middle magnetosphere currents and auroral precipitation by solar wind-induced compressions and expansions of the magnetosphere: initial response and steady state. *Planetary and Space Science*, *51*(1), 31–56. Retrieved from https://doi.org/10.1016/s0032-0633(02)00130-7

Cowley, S. W. H., Nichols, J. D., & Andrews, D. J. (2007, June). Modulation of jupiter's plasma flow, polar currents, and auroral precipitation by solar wind-induced compressions and expansions of the magnetosphere: a simple theoretical model. *Annales Geophysicae*, *25*(6), 1433–1463. Retrieved from https://doi.org/10.5194/angeo-25-1433-2007

Cowley, S. W. H., Nichols, J. D., & Bunce, E. J. (2002). Distributions of current and auroral precipitation in jupiter's middle magnetosphere computed from steady-state hill–pontius angular velocity profiles: solutions for current sheet and dipole magnetic field models. *Planetary and Space Science*, *50*(7-8), 717–734. Retrieved from https://doi.org/10.1016/s0032-0633(02)00046-6

Hill, T. W. (1979). Inertial limit on corotation. *Journal of Geophysical Research*, *84*(A11), 6554. doi: 10.1029/ja084ia11p06554

Hill, T. W. (2001). The jovian auroral oval. *Journal of Geophysical Research: Space Physics*, *106*(A5), 8101–8107. Retrieved from https://doi.org/10.1029/2000ja000302

Joy, S. P. (2002). Probabilistic models of the Jovian magnetopause and bow shock locations. *Journal of Geophysical Research*, *107*(A10). Retrieved from https://doi.org/10.1029/2001ja009146

Khurana, K. K. (2005). Global structure of jupiter's magnetospheric current sheet. *Journal of Geophysical Research*, *110*(A7). Retrieved from https://doi.org/10.1029/2004ja010757

Lorch, C. T. S., Ray, L. C., Arridge, C. S., Khurana, K. K., Martin, C. J., & Bader, A. (2020). Local time asymmetries in jupiter's magnetodisc currents. *Journal of Geophysical Research: Space Physics*, *125*(2). Retrieved from https://doi.org/10.1029/2019ja027455

Louarn, P., Kivelson, M. G., & Kurth, W. S. (2016, October). On the links between the radio flux and magnetodisk distortions at jupiter. *Journal of Geophysical Research: Space Physics*, *121*(10), 9651–9670. Retrieved from https://doi.org/10.1002/2016ja023106

Nichols, J. D. (2011). Magnetosphere-ionosphere coupling in Jupiter's middle magnetosphere: Computations including a self-consistent current sheet magnetic field model. *Journal of Geophysical Research: Space Physics*, *116*(A10).

Nichols, J. D., Achilleos, N., & Cowley, S. W. H. (2015). A model of force balance in Jupiter's magnetodisc including hot plasma pressure anisotropy. *Journal of Geophysical Research: Space Physics*, *120*(12), 10,185-10,206. Retrieved from https://doi.org/10.1002/2015ja021807

Nichols, J. D., Allegrini, F., Bagenal, F., Bunce, E. J., Cowley, S. W. H., Ebert, R. W., ... Yao, Z. (2020, August). An enhancement of jupiter's main auroral emission and magnetospheric currents. *Journal of Geophysical Research: Space Physics*, *125*(8). Retrieved from https://doi.org/10.1029/2020ja027904

Nichols, J. D., & Cowley, S. W. H. (2003). Magnetosphere-ionosphere coupling currents in jupiter's middle magnetosphere: dependence on the effective ionospheric pedersen conductivity and iogenic plasma mass outflow rate. *Annales Geophysicae*, *21*(7), 1419–1441. Retrieved from https://doi.org/10.5194/angeo-21-1419-2003

Nichols, J. D., & Cowley, S. W. H. (2004). Magnetosphere-ionosphere coupling currents in jupiter's middle magnetosphere: effect of precipitation-induced enhancement of the ionospheric pedersen conductivity. *Annales Geophysicae*, *22*(5), 1799–1827. Retrieved from https://doi.org/10.5194/angeo-22-1799-2004

Nichols, J. D., & Cowley, S. W. H. (2005, March). Magnetosphere-ionosphere coupling currents in jupiter's middle magnetosphere: effect of magnetosphere-ionosphere decoupling by field-aligned auroral voltages. *Annales Geophysicae*, *23*(3), 799–808. Retrieved from https://doi.org/10.5194/angeo-23-799-2005

Pensionerov, I. A., Alexeev, I. I., Belenkaya, E. S., Connerney, J. E. P., & Cowley, S. W. H. (2019). Model of jupiter's current sheet with a piecewise current density. *Journal of Geophysical Research: Space Physics*, *124*(3), 1843–1854. Retrieved from https://doi.org/10.1029/2018ja026321

Pontius, D. H. (1997). Radial mass transport and rotational dynamics. *Journal of Geophysical Research: Space Physics*, *102*(A4), 7137–7150. Retrieved from https://doi.org/10.1029/97ja00289

Ray, L. C., Achilleos, N. A., Vogt, M. F., & Yates, J. N. (2014, June). Local time variations in jupiter's magnetosphere-ionosphere coupling system. *Journal of Geophysical Research: Space Physics*, *119*(6), 4740–4751. Retrieved from https://doi.org/10.1002/2014ja019941

Ray, L. C., Achilleos, N. A., & Yates, J. N. (2015, August). The effect of including field-aligned potentials in the coupling between jupiter's thermosphere, ionosphere, and magnetosphere. *Journal of Geophysical Research: Space Physics*, *120*(8), 6987–7005. Retrieved from https://doi.org/10.1002/2015ja021319

Ray, L. C., Ergun, R. E., Delamere, P. A., & Bagenal, F. (2010, September). Magnetosphere-ionosphere coupling at jupiter: Effect of field-aligned potentials on angular momentum transport. *Journal of Geophysical Research: Space Physics*, *115*(A9), n/a–n/a. Retrieved from https://doi.org/10.1029/2010ja015423

Tao, C., Fujiwara, H., & Kasaba, Y. (2009, August). Neutral wind control of the jovian magnetosphere-ionosphere current system. *Journal of Geophysical Research: Space Physics*, *114*(A8), n/a–n/a. Retrieved from https://doi.org/10.1029/2008ja013966

Tao, C., Fujiwara, H., & Kasaba, Y. (2010, February). Jovian magnetosphere–ionosphere current system characterized by diurnal variation of ionospheric conductance. *Planetary and Space Science*, *58*(3), 351–364. Retrieved from https://doi.org/10.1016/j.pss.2009.10.005

Vasyliunas, V. M. (1983). Plasma distribution and flow. In *Physics of the jovian magnetosphere* (pp. 395–453). Cambridge University Press. Retrieved from https://doi.org/10.1017/cbo9780511564574.013

Vogt, M. F., Kivelson, M. G., Khurana, K. K., Walker, R. J., Bonfond, B., Grodent, D., & Radioti, A. (2011, March). Improved mapping of jupiter's auroral features to magnetospheric sources. *Journal of Geophysical Research: Space Physics*, *116*(A3). Retrieved from https://doi.org/10.1029/2010ja016148